NANO LETTERS

Letter

pubs.acs.org/NanoLett

Electric-Field Induced Activation of Dark Excitonic States in Carbon Nanotubes

T. Uda, M. Yoshida, A. Ishii, and Y. K. Kato*

Institute of Engineering Innovation, The University of Tokyo, Tokyo 113-8656, Japan

Supporting Information

ABSTRACT: Electrical activation of optical transitions to parity-forbidden dark excitonic states in individual carbon nanotubes is reported. We examine electric-field effects on various excitonic states by simultaneously measuring photocurrent and photoluminescence. As the applied field increases, we observe an emergence of new absorption peaks in the excitation spectra. From the diameter dependence of the energy separation between the new peaks and the ground state of E_{11} excitons, we attribute the peaks to the dark excited states which became optically active due to the applied field. Field-induced exciton dissociation can explain the photocurrent threshold field, and the edge of the E_{11} continuum states has been identified by extrapolating to zero threshold.

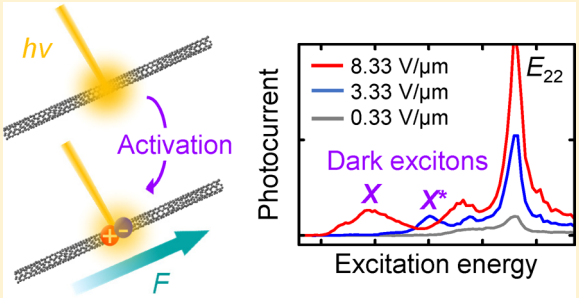

KEYWORDS: *Carbon nanotubes, photocurrent, photoluminescence, dark excitons, exciton dissociation, field-effect transistors*

The rich physical properties of single-walled carbon nanotubes make them a promising material for nanoscale photonic and optoelectronic devices,[1] and therefore manipulation of their optical transitions has important implications. The strong Coulomb interactions due to the limited screening in quasi-one-dimensional systems result in optical spectra dominated by tightly bound excitons with binding energies of more than a few hundred meV.[2−5] These excitons have a series of excited states in a manner similar to the Rydberg states in atomic hydrogen, and they have either odd (u) or even (g) parity because of the K and K′ valleys in the momentum space being equivalent.[5−8] Since one-photon transitions require a parity change, the odd excitonic series ($1u$, $2u$, $3u$, ...) are bright, while the even excitonic series ($1g$, $2g$, $3g$, ...) are dipole-forbidden dark states.[6−8]

These dark states have been studied by two-photon excitation spectroscopy that allows for same-parity transitions,[4,6,8] and photoluminescence (PL) measurements under strong magnetic fields have been used as well.[9−12] It is expected that electric fields also cause the dark states to become optically active because of wave function mixing,[13] and it gives rise to interesting phenomena such as exciton dissociation, Stark shift, and Franz−Keldysh oscillations.[14−21] In particular, the activation of the dark states could be a key to developing efficient nanotube-based photodetectors and photovoltaic devices, but a well-controlled experiment has been lacking. Although electroabsorption spectra have been interpreted by state-mixing effects,[22] complicated spectra for an ensemble of nanotubes result in large uncertainties. Spectral diffusion has been attributed to impurity-induced fields,[23] while their fluctuating nature makes it difficult to draw quantitative conclusions.

Here we report on the electrical activation of the parity-forbidden dark excitonic states in individual carbon nanotubes. By simultaneously measuring both photocurrent (PC) and PL, electric-field effects on excited excitonic states are investigated. When the applied field is increased, we observe an emergence of new absorption peaks in PC spectra at energies near the bright excited states. By measuring several nanotubes with different chiralities, the energy separation between these bias-induced peaks and the $1u$ state of E_{11} excitons is found to be inversely proportional to the tube diameter. The results show that the new peaks are the $2g$ and $3g$ dark excited states of the E_{11} excitons which became optically active due to the applied fields. Furthermore, we find that a field-induced exciton dissociation model can explain the PC threshold fields, and a spectral feature that corresponds to zero threshold is interpreted as the edge of the continuum states.

The measurements are performed on air-suspended nanotube field-effect transistors,[14,19,24] and fabrication starts by forming trenches on Si substrates with 300-nm-thick oxide using electron beam lithography and dry etching. Another lithography step defines the source and drain electrodes on both sides of the trenches, and an electron beam evaporator is used to deposit 1 nm Ti and 30 nm Pt. Finally, nanotubes are grown over the trenches by chemical vapor deposition with patterned catalyst.[19,25,26] A schematic of a device is shown in the inset of Figure 1b.

Simultaneous PC and PL measurements are performed with a home-built sample scanning microscopy system.[27] Wave-

Received: November 11, 2015
Revised: February 4, 2016
Published: March 21, 2016

DOI: 10.1021/acs.nanolett.5b04595
Nano Lett. 2016, 16, 2278−2282

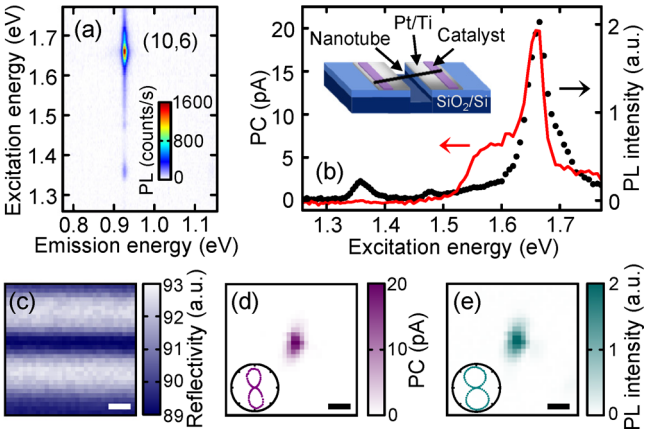

Figure 1. Optical characterization of a (10,6) nanotube in a device with w = 0.6 μm. Excitation power is 10 μW, and laser polarization is parallel to the nanotubes axis unless otherwise noted. (a) A PL excitation map measured with F = 0.00 V/μm. (b) PC (red curve) and PL (black dots) excitation spectra. PL intensity is obtained by fitting the emission spectra with Lorentzian functions and calculating the peak area. Inset is a schematic of the device. (c), (d), and (e) are reflectivity, PC, and PL images, respectively. The scale bars are 1 μm. Insets in (d) and (e) are the laser polarization angle dependence of the PC and PL intensity, respectively. (c–e) are measured at an excitation energy of 1.66 eV. (b–e) are measured at F = 0.33 V/μm. We note that PL polarization dependence is less pronounced compared to PC because of exciton–exciton annihilation effects.[14,27,28]

length tunable Ti:sapphire laser is used for excitation, and an objective lens with a numerical aperture of 0.8 and a working distance of 3.4 mm focuses the laser onto the sample. The linear polarization of the laser can be rotated using a half-wave plate placed immediately before the lens, and an optical chopper in the excitation path modulates the laser intensity at 683 Hz. We use a lock-in amplifier to eliminate low-frequency noise and to achieve sensitive detection of PC. The source contact is connected to a virtual ground input of the lock-in, and a bias voltage V is applied to the drain contact to establish an electric field $F = V/w$ where w is the width of the trench.[19] In order to avoid PL quenching caused by electrostatic doping,[24,26] we also apply $V/2$ to the Si substrate to keep the effective gate voltage at the center of the tube to be zero.[14] PL is collected through a confocal pinhole, and an InGaAs photodiode array attached to a spectrometer is used for detection. All measurements are carried out at room temperature in air.

When a PL signal from a nanotube is observed, we first perform PL excitation spectroscopy at F = 0.00 V/μm to determine its chirality. In Figure 1a, a PL excitation map for a nanotube in a typical device is shown, where an excitation laser power P = 10 μW is used. We assign the chirality by comparing the E_{11} and E_{22} energies to tabulated data[27] and confirm that both of the values differ by less than 10 meV. Simultaneously measured PC and PL excitation spectra (Figure 1b) at a low electric field of F = 0.33 V/μm confirm that the E_{22} absorption resonance occurs at an identical energy of 1.66 eV, while imaging measurements (Figure 1c–e) ensure that both signals are spatially coincident at the trench. Polarization dependence (Figure 1d,e insets) is used to determine the angle of the nanotube,[28] and we confirm that both PC and PL show consistent behavior. These procedures ensure that the signals arise from the same individual nanotube.

After such careful characterization, electric field dependence of PC and PL excitation spectra are investigated (Figure 2).

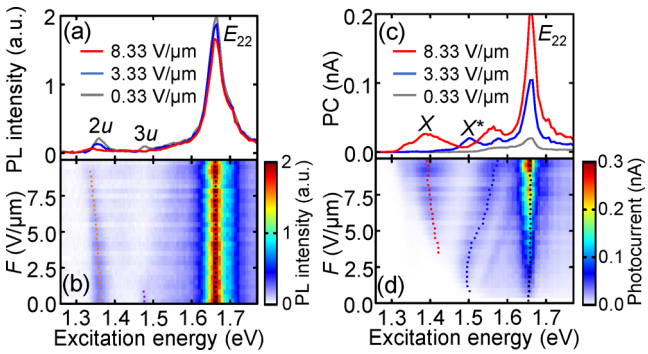

Figure 2. Nanotube characterized in Figure 1 measured with P = 10 μW. The laser polarization is parallel to the nanotubes axis. (a) and (c) are PL excitation and PC spectra, respectively, measured at F = 0.33 V/μm (gray), F = 3.33 V/μm (blue), and F = 8.33 V/μm (red). (b) and (d) are electric field dependence of PL excitation and PC spectra, respectively, taken from F = 0.00 to 10.00 V/μm with 0.33 V/μm step. The orange, purple, red, blue, and black dots indicate spectral peak positions for the 2u, 3u, X, X*, and E_{22}, respectively.

Three PL excitation spectra measured at different electric fields are shown in Figure 2a, and a more detailed electric field dependence taken from F = 0.00 to 10.00 V/μm is shown in Figure 2b. The most prominent peak observed at 1.66 eV corresponds to the E_{22} exciton ground state, which does not show much field dependence. In the spectrum obtained at F = 0.33 V/μm (Figure 2a, gray curve), we observe two weaker peaks at 1.36 and 1.48 eV which can be assigned to the 2u and 3u states, respectively.[5,6] When the applied electric field is increased to F = 3.33 V/μm, the peak for the 3u state disappears (Figure 2a, blue curve), and with a further increase to F = 8.33 V/μm, the peak for the 2u state shows a redshift and a considerable reduction in its height (Figure 2a, red curve). The behaviors of 2u and 3u states are much more sensitive to the electric field, in contrast to the E_{22} exciton peak.

In PC spectra, more significant changes are observed (Figure 2c,d). Under the weakest electric field of F = 0.33 V/μm, only the E_{22} exciton ground state is observed (Figure 2c, gray curve). When the applied electric field is increased to F = 3.33 V/μm, a new peak appears at 1.50 eV (Figure 2c, blue curve). This peak is close to but different from the 3u state (see Figure S1 in the Supporting Information) and is denoted as X* in Figure 2c. As the electric field is increased (Figure 2d), we observe a blueshift of the X* peak and an emergence of another lower energy peak which we will refer to as the X peak. At F = 8.33 V/μm, the X* peak and the X peak can be seen at 1.56 and 1.39 eV, respectively (Figure 2c, red curve). We note that the X peak can also be observed in the PL excitation spectra as a faint peak (Figure 2b, Figure S2 in the Supporting Information).

A conceivable explanation for the X and X* peaks is that they are the parity-forbidden dark excited states. Since electric fields cause wave function mixing,[13,22,23] the dark states can become optically active. If these states dissociate into free carriers by the field, peaks can appear in the PC spectra. The X and X* peaks show up near the 2u and 3u states, suggesting that they correspond to the 2g and 3g states, respectively.

In order to examine if such a picture is reasonable, a more detailed quantitative analysis is performed. We fit each peak in the PL excitation and PC spectra in Figure 2b,d by using a

DOI: 10.1021/acs.nanolett.5b04595
Nano Lett. 2016, 16, 2278–2282

Lorentzian plus a linear function and plot the electric field dependence of the peak heights and positions in Figure 3. First

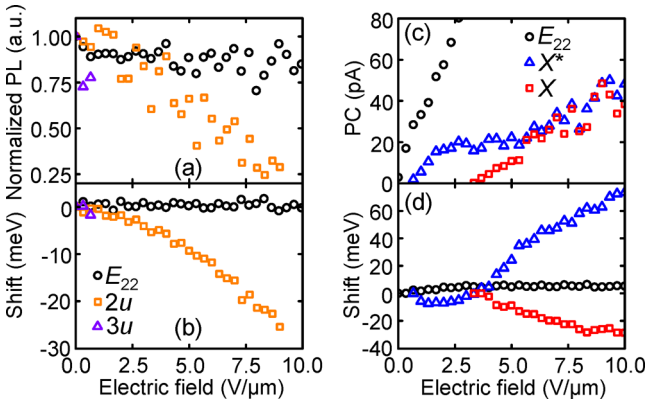

Figure 3. Fitting results of various peaks in Figure 2b,d by using a Lorentzian plus a linear function. (a and c) Electric field dependence of peak heights in the PL excitation and PC spectra, respectively. For (a), PL intensities are normalized at $F = 0.00$ V/μm. (b and d) Electric field dependence of energy shifts for the peaks in the PL excitation and PC spectra, respectively. The shifts for the E_{22}, 2u, 3u, X^*, and X are measured from 1.662, 1.361, 1.477, 1.502, and 1.421 eV, respectively.

we discuss the changes in the normalized PL intensity (Figure 3a). As the field increases to $F = 10.00$ V/μm, E_{22} excitation results in only about 20% decrease while 2u-state excitation shows a reduction to about one-quarter, again highlighting the sensitivity of the excited states to electric fields. In the electric field dependence of the peak PC, different dissociation behaviors are observed for the various peaks (Figure 3c). PC increases linearly without a threshold for E_{22} excitation, indicating that built-in electric fields are negligible and excitons are spontaneously dissociating.[14] In the case of X and X^* peaks, however, we observe thresholds at $F = 3.33$ V/μm and 0.67 V/μm, respectively, showing that electric fields are necessary for dissociation of the underlying states. The X^* peak shows a higher PC compared to the X peak, which may be due to either larger absorption cross section or more efficient dissociation.

Next we discuss the energy shifts of the peaks in the PL excitation and PC spectra (Figure 3b,d). The peak position of the E_{22} excitons do not shift so much which is similar to the behavior of 1u state of E_{11} excitons,[19] while the 2u state shows a large Stark shift of about 30 meV at $F = 10.00$ V/μm. This is expected as the excited states generally have larger sizes compared to the ground states, and therefore they are more responsive to the applied field. Similar to the 2u state, the X and X^* peaks also show large shifts of about 30 and 70 meV, respectively, consistent with the interpretation that the X and X^* peaks are the excited states. We note that the dispersions of the peak shifts show different behaviors, which may be caused by complicated mixing of various excitonic states such as K-momentum states and the E_{22} state as well as the E_{11} continuum.

To obtain additional data that support the assignment of the X and X^* peaks, we perform PC and PL excitation measurements on various individual nanotubes with different chiralities. Three typical PC spectra that show the X peaks are plotted in Figure 4a–c. No correlation between the X and E_{22} peaks are observed, showing that they are not a sideband of E_{22} excitons. We fit such spectra using Lorentzian functions and plot the energy difference between the various peaks and the 1u

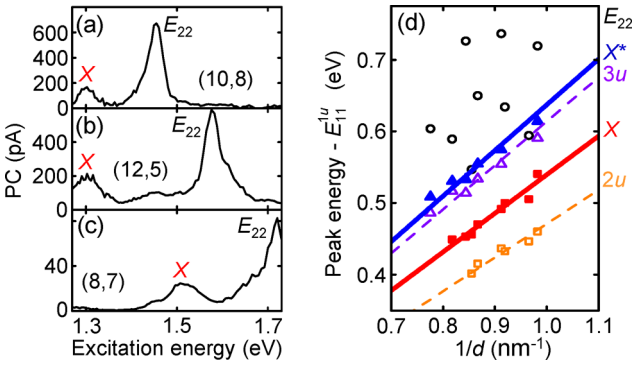

Figure 4. (a) PC spectrum for a (10,8) nanotube measured with $F = 5.94$ V/μm and $P = 10$ μW. (b) PC spectrum for a (12,5) nanotube measured with $F = 8.75$ V/μm and $P = 10$ μW. (c) PC spectrum for a (8,7) nanotube measured with $F = 11.67$ V/μm and $P = 5$ μW. (d) Diameter dependence of the energy separation from the 1u states for 2u (orange open squares), X (red filled squares), X^* (blue filled triangles), 3u (purple open triangles), and E_{22} (black open circles). The X and X^* peak positions are identified using PC spectra at the weakest electric field where they can be observed. Typical fields are $F = 5.0$ and 1.5 V/μm for the X and X^* peaks, respectively. For the bright excitonic states, PL excitation spectra taken with $F < 0.20$ V/μm are used. Lines show linear fits with zero intercept, and the slopes are 471, 540, 614, and 637 meV·nm for 2u, X, 3u, and X^*, respectively.

state as a function of the tube diameter d in Figure 4d. The energy separations for the bright excited states (2u and 3u states) are inversely proportional to d, as observed previously.[5] The inverse proportionality is a characteristic of the excited states,[29] and similar dependence has also been observed for the 2g states.[30] We find that the X and X^* peaks also show such a dependence, indicating that the peaks arise from the excited states of E_{11} excitons. It is noted that these peaks cannot be observed in the absence of the electric fields, for all of the chiralities investigated. In addition, the X peak always appears at an energy higher than the 2u state but lower than the 3u state, and the X^* peak shows up slightly above the 3u state for all nanotubes. These results confirm our interpretation that the X and X^* peaks are the 2g and 3g states of E_{11} excitons, respectively.

The assignment is consistent with previous work on the dark states that used micelle-wrapped tubes. The 2u states are observed at 200 meV above the 1u states by one-photon measurements, while two-photon excitation measurements have shown that the energy difference between the 2g states and the 1u states is 240 meV.[6] Since our nanotubes are air-suspended and environmental dielectric screening is weaker, enhancement of the energy separation is expected.[31,32] Indeed, we observe the 2u states and the 2g states (X peaks) at 470 and 540 meV above the 1u states, respectively, for $d = 1.00$ nm tubes (Figure 4d). These results are consistent with the dielectric constant scaling obtained for air-ambient nanotubes.[5] Note that the X peaks are typically identified at $F = 5.0$ V/μm where redshifts of about 20 meV have occurred. Taking into account such shifts, the ratio of the energy separations is comparable to the micelle-wrapped tubes.

We now turn our attention to PC threshold fields for the 2g (X) and 3g (X^*) states (Figure 3c) and show that they can be explained by field-induced exciton dissociation. In the presence of electric fields, bound excitons can tunnel into the continuum, and the dissociation threshold field scales as $E_b^{3/2}$ where E_b is the exciton binding energy.[20] The relatively large threshold field

DOI: 10.1021/acs.nanolett.5b04595
Nano Lett. 2016, 16, 2278–2282

observed for the $2g$ (X) state can be attributed to its lager binding energy, and in general excited states farther away from the continuum should show higher thresholds. Indeed, in Figure 2d, the boundary between the blue region and the white region shows such a dependence as expected (also see Figure S3 in the Supporting Information). The dissociation mechanism is similar to the ionization of a hydrogen atom in a field,[33] but with binding energies that is 2 orders of magnitude smaller. In comparison to bulk semiconductors, the ground state binding energy is more than an order of magnitude larger, allowing for spectroscopic study of the excited states.

Based on this analysis, we consider the point where the dissociation field becomes zero which should correspond to the edge of the continuum states. For the tube shown in Figure 2d, it is located at 1.55 eV, and the PC spectrum measured at the lowest electric field (Figure 1b) shows a shoulder above this energy. As the excited states of E_{11} excitons are lower in energy compared to the shoulder, it is reasonable to interpret this spectral feature as the E_{11} continuum states. Similar features are observed in other nanotubes with different chiralities (Figure 5), supporting the interpretation. We note that the continuum states can only be observed clearly in certain chiralities whose E_{22} excitons are sufficiently separated from the continuum edge. The direct identification of the continuum edge has been difficult in carbon nanotubes because most of the oscillator strength is transferred to excitonic resonances. In spite of such an effect, PC spectroscopy provides a way to determine the edge because of the zero dissociation fields.

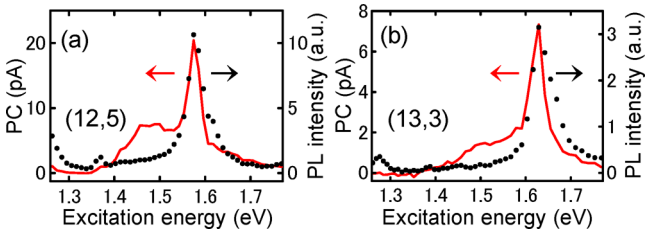

Figure 5. PC (red curve) and PL excitation (black dots) spectra obtained at low electric fields, which show the continuum states as shoulders. (a) Spectra for a (12,5) nanotube measured with F = 0.13 V/μm and P = 10 μW. (b) Spectra for a (13,3) nanotube measured with F = 0.10 V/μm and P = 10 μW.

In summary, we have investigated the electric field dependence of various excitonic states in individual suspended carbon nanotubes by simultaneously measuring both PC and PL. As fields are increased, optical transitions to the parity-forbidden dark states of E_{11} excitons are activated. The clear diameter dependence of the peak energies has been used to assign them to the $2g$ and $3g$ states. Furthermore, we have observed PC threshold fields that can be explained by field-induced exciton dissociation, and a shoulder in the PC spectra have been identified as the E_{11} continuum states. Our findings show the strong influence of electric fields on the excited states of excitons, and may lead to nanoscale optoelectronic devices that utilize the dark excitonic states.

■ ASSOCIATED CONTENT

Supporting Information

The Supporting Information is available free of charge on the ACS Publications website at DOI: 10.1021/acs.nanolett.5b04595.

Additional PC and PL excitation spectra measured with P = 100 μW (PDF)

■ AUTHOR INFORMATION

Corresponding Author

*E-mail: ykato@sogo.t.u-tokyo.ac.jp. Phone: +81-3-5841-7702. Fax: +81-3-5841-7772.

Notes

The authors declare no competing financial interest.

■ ACKNOWLEDGMENTS

We thank T. Kan and I. Shimoyama for the use of the evaporator and S. Yamamoto for the plasma etcher. This work was supported by JSPS (KAKENHI 24340066, 26610080), MEXT (Photon Frontier Network Program, Nanotechnology Platform), Canon Foundation, and Asahi Glass Foundation. The samples were fabricated at the Center for Nano Lithography & Analysis at The University of Tokyo. T.U. and M.Y. are supported by JSPS (ALPS), and A.I. is supported by JSPS (MERIT, Research Fellowship for Young Scientists).

■ REFERENCES

(1) Avouris, P.; Freitag, M.; Perebeinos, V. *Nat. Photonics* **2008**, *2*, 341−350.
(2) Ogawa, T.; Takagahara, T. *Phys. Rev. B: Condens. Matter Mater. Phys.* **1991**, *44*, 8138−8156.
(3) Ando, T. *J. Phys. Soc. Jpn.* **1997**, *66*, 1066−1073.
(4) Wang, F.; Dukovic, G.; Brus, L. E.; Heinz, T. F. *Science* **2005**, *308*, 838−841.
(5) Lefebvre, J.; Finnie, P. *Nano Lett.* **2008**, *8*, 1890−1895.
(6) Maultzsch, J.; Pomraenke, R.; Reich, S.; Chang, E.; Prezzi, D.; Ruini, A.; Molinari, E.; Strano, M. S.; Thomsen, C.; Lienau, C. *Phys. Rev. B: Condens. Matter Mater. Phys.* **2005**, *72*, 241402.
(7) Barros, E. B.; Capaz, R. B.; Jorio, A.; Samsonidze, G. G.; Souza Filho, A. G.; Ismail-Beigi, S.; Spataru, C. D.; Louie, S. G.; Dresselhaus, G.; Dresselhaus, M. S. *Phys. Rev. B: Condens. Matter Mater. Phys.* **2006**, *73*, 241406.
(8) Kimoto, Y.; Okano, M.; Kanemitsu, Y. *Phys. Rev. B: Condens. Matter Mater. Phys.* **2013**, *87*, 195416.
(9) Zaric, S.; Ostojic, G. N.; Kono, J.; Shaver, J.; Moore, V. C.; Strano, M. S.; Hauge, R. H.; Smalley, R. E.; Wei, X. *Science* **2004**, *304*, 1129−1131.
(10) Mortimer, I. B.; Nicholas, R. J. *Phys. Rev. Lett.* **2007**, *98*, 027404.
(11) Shaver, J.; Kono, J.; Portugall, O.; Krstic, V.; Rikken, G. L. J. A.; Miyauchi, Y.; Maruyama, S.; Perebeinos, V. *Nano Lett.* **2007**, *7*, 1851−1855.
(12) Matsunaga, R.; Matsuda, K.; Kanemitsu, Y. *Phys. Rev. Lett.* **2008**, *101*, 147404.
(13) Zhao, H.; Mazumdar, S. *Phys. Rev. Lett.* **2007**, *98*, 166805.
(14) Kumamoto, Y.; Yoshida, M.; Ishii, A.; Yokoyama, A.; Shimada, T.; Kato, Y. K. *Phys. Rev. Lett.* **2014**, *112*, 117401.
(15) Barkelid, M.; Zwiller, V. *Nat. Photonics* **2014**, *8*, 47−51.
(16) Kazaoui, S.; Cook, S.; Izard, N.; Murakami, Y.; Maruyama, S.; Minami, N. *J. Phys. Chem. C* **2014**, *118*, 18059−18063.
(17) Park, J.; Reid, O. G.; Blackburn, J. L.; Rumbles, G. *Nat. Commun.* **2015**, *6*, 8809.
(18) Mohite, A. D.; Gopinath, P.; Shah, H. M.; Alphenaar, B. W. *Nano Lett.* **2008**, *8*, 142−146.
(19) Yoshida, M.; Kumamoto, Y.; Ishii, A.; Yokoyama, A.; Kato, Y. K. *Appl. Phys. Lett.* **2014**, *105*, 161104.
(20) Perebeinos, V.; Avouris, P. *Nano Lett.* **2007**, *7*, 609−613.
(21) Ham, M. H.; Kong, B. S.; Kim, W. J.; Jung, H. T.; Strano, M. S. *Phys. Rev. Lett.* **2009**, *102*, 047402.
(22) Kishida, H.; Nagasawa, Y.; Imamura, S.; Nakamura, A. *Phys. Rev. Lett.* **2008**, *100*, 097401.

DOI: 10.1021/acs.nanolett.5b04595
Nano Lett. 2016, 16, 2278−2282

(23) Matsuda, K.; Inoue, T.; Murakami, Y.; Maruyama, S.; Kanemitsu, Y. *Phys. Rev. B: Condens. Matter Mater. Phys.* **2008**, *77*, 193405.
(24) Yasukochi, S.; Murai, T.; Moritsubo, S.; Shimada, T.; Chiashi, S.; Maruyama, S.; Kato, Y. K. *Phys. Rev. B: Condens. Matter Mater. Phys.* **2011**, *84*, 121409(R).
(25) Yokoyama, A.; Yoshida, M.; Ishii, A.; Kato, Y. K. *Phys. Rev. X* **2014**, *4*, 011005.
(26) Jiang, M.; Kumamoto, Y.; Ishii, A.; Yoshida, M.; Shimada, T.; Kato, Y. K. *Nat. Commun.* **2015**, *6*, 6335.
(27) Ishii, A.; Yoshida, M.; Kato, Y. K. *Phys. Rev. B: Condens. Matter Mater. Phys.* **2015**, *91*, 125427.
(28) Moritsubo, S.; Murai, T.; Shimada, T.; Murakami, Y.; Chiashi, S.; Maruyama, S.; Kato, Y. K. *Phys. Rev. Lett.* **2010**, *104*, 247402.
(29) Ando, T. *J. Phys. Soc. Jpn.* **2009**, *78*, 104703.
(30) Dukovic, G.; Wang, F.; Song, D.; Sfeir, M. Y.; Heinz, T. F.; Brus, L. E. *Nano Lett.* **2005**, *5*, 2314−2318.
(31) Perebeinos, V.; Tersoff, J.; Avouris, P. *Phys. Rev. Lett.* **2004**, *92*, 257402.
(32) Lefebvre, J.; Finnie, P. *Phys. Rev. Lett.* **2007**, *98*, 167406.
(33) Bethe, H. A.; Salpeter, E. E. *Quantum Mechanics of One- and Two- Electron Atoms*; Springer-Verlag: Berlin, 1957.

DOI: 10.1021/acs.nanolett.5b04595
Nano Lett. 2016, 16, 2278−2282